

# Exploiting Temporal Contexts with Strided Transformer for 3D Human Pose Estimation

Wenhao Li, Hong Liu<sup>†</sup>, Runwei Ding, Mengyuan Liu, Pichao Wang, and Wenming Yang

**Abstract**—Despite great progress in 3D human pose estimation from videos, it is still an open problem to take full advantage of redundant 2D pose sequences to learn representative representation for generating one single 3D pose. To this end, we propose an improved Transformer-based architecture, called Strided Transformer, for 3D human pose estimation in videos to lift a sequence of 2D joint locations to a 3D pose. Specifically, a vanilla Transformer encoder (VTE) is adopted to model long-range dependencies of 2D pose sequences. To reduce redundancy of the sequence and aggregate information from local context, strided convolutions are incorporated into VTE to progressively reduce the sequence length. The modified VTE is termed as strided Transformer encoder (STE) which is built upon the outputs of VTE. STE not only effectively aggregates long-range information to a single-vector representation in a hierarchical global and local fashion but also significantly reduces the computation cost. Furthermore, a full-to-single supervision scheme is designed at both the full sequence scale and single target frame scale, applied to the outputs of VTE and STE, respectively. This scheme imposes extra temporal smoothness constraints in conjunction with the single target frame supervision and improves the representation ability of features for the target frame. The proposed architecture is evaluated on two challenging benchmark datasets, Human3.6M and HumanEva-I, and achieves state-of-the-art results with much fewer parameters.

**Index Terms**—3D human pose estimation, Transformer, strided convolution.

## I. INTRODUCTION

3D human pose estimation aims to estimate 3D joint locations of a human body from images or videos. This task has drawn tremendous attention in the past decades [1]–[4], with wide applications in computer animation [5], action understanding [6]–[9], and human-robot interactions [10], [11]. Many state-of-the-art approaches adopt a two-stage pipeline [12]–[14], which first estimates 2D keypoints and then lifts them to the 3D space. However, it is still an ill-posed problem due to depth ambiguity, since multiple 3D interpretations can map to the same 2D keypoints from monocular images.

<sup>†</sup> Corresponding author.

W. Li, H. Liu, and R. Ding are with Key Laboratory of Machine Perception, Shenzhen Graduate School, Peking University, Beijing 100871, China. E-mail: {wenhaoli, hongliu, dingrunwei}@pku.edu.cn. M. Liu is with School of Intelligent Systems Engineering, Sun Yat-sen University, China. E-mail: nkliuyifang@gmail.com. P. Wang is with Alibaba Group, Bellevue, WA, 98004, USA. E-mail: pichao.wang@alibaba-inc.com. W. Yang is with the Shenzhen Key Lab of Information Science and Technology, Shenzhen Engineering Lab of IS&DRM, Department of Electronic Engineering, Graduate School at Shenzhen, Tsinghua University, Shenzhen 518055, China. E-mail: yang.wenming@sz.tsinghua.edu.cn

This work is supported by National Key R&D Program of China (No. 2020AAA0108904), Basic and Applied Basic Research Foundation of Guangdong (No. 2020A1515110370), Science and Technology Plan of Shenzhen (Nos. JCYJ20190808182209321, JCYJ20200109140410340).

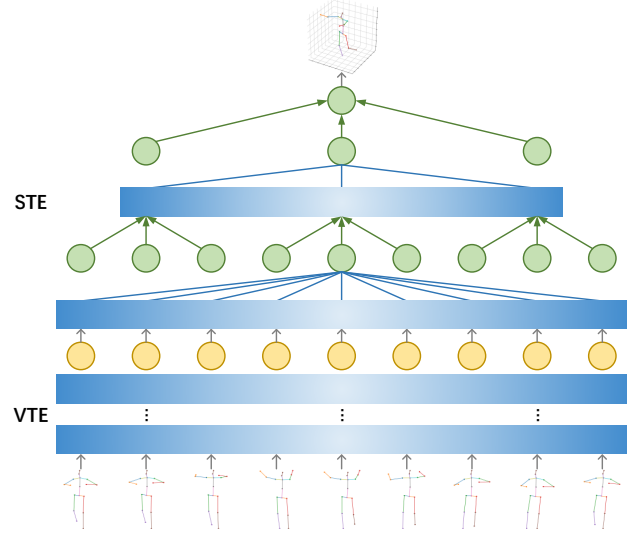


Fig. 1: Our strided Transformer encoder (STE) takes outputs of vanilla Transformer encoder (VTE) as input (yellow) and generates a 3D pose for the target frame as output (top). The self-attention mechanism (blue) concentrates on global context and strided convolution (green) aggregates information from local context.

To alleviate this problem, temporal context information has been investigated by many researchers. Some methods [15]–[17] leverage past and future data in the sequence to predict the 3D pose of the target frame. For instance, Cai *et al.* [17] presented a local-to-global graph convolutional network to exploit spatial-temporal relations to estimate 3D poses from a sequence of skeletons. However, these approaches have small temporal receptive fields and limited temporal correlation windows, thus suffering from modeling long-term dependencies.

Therefore, the first question is, which architecture can effectively model long-term dependencies, thereby benefiting from a large receptive field to capture richer depth information? Vanilla Transformer [18] is developed for exploiting long-range dependencies and achieves tremendous success in natural language processing [19], [20] and computer vision [21]–[25]. It consists of self-attention module and position-wise feed-forward network (FFN). The self-attention module computes pairwise dot-product between all input elements to capture global-context information and the FFN acts as pattern detectors over the input across all layers [26]. Such design looks quite suitable for the 2D-3D pose lifting method to

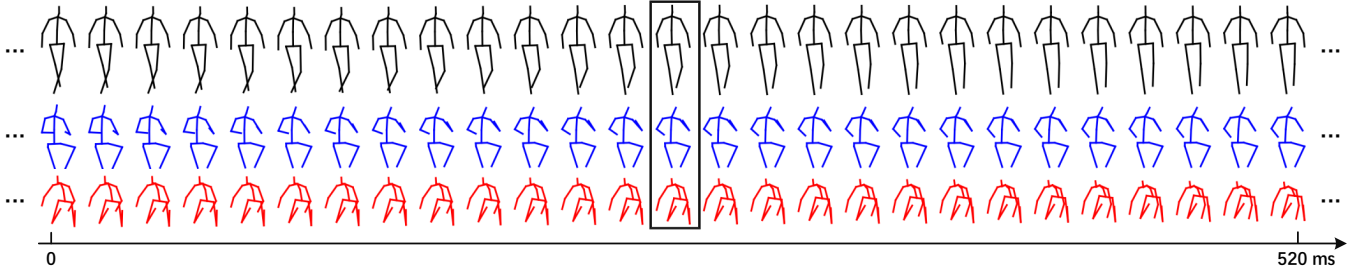


Fig. 2: Example of 2D pose sequences of 27 consecutive frames (520 ms) on Human3.6M dataset (captured from 50 Hz cameras). It contains much redundant information as nearby poses are same. The rectangle denotes the center frames.

capture long-range dependencies. However, is the design of pure Transformer architecture a good choice for video-based 3D human pose estimation?

To answer this question, we first analyze the shortcomings of pure Transformer architecture, *i.e.*, vanilla Transformer encoder (VTE) [18]: (i) The full-length sequence of hidden representations in VTE actually contains significant redundancy for video-based pose estimation, as nearby poses are quite similar, illustrated in Fig. 2. (ii) When a long sequence is input to the VTE, the computation of attention layers grows quadratically, which requires extremely high computational resources. And the receptive field is often forced to be reduced due to constrained resources and consideration of practical applications while a large receptive field is crucial to enhance the estimation consistency [27]. (iii) VTE architecture may neglect local contexts, but the utilization of local information is crucial in computer vision tasks. To overcome these issues, we propose to gradually merge nearby poses to reduce the sequence length till to one target pose representation. An alternative is to perform the pooling operation after the FFN [20]. However, lots of valuable information may be lost if using pooling operation, and the local information can not be well exploited. Inspired by previous methods [13], [27] that take temporal convolutions to handle sequences with different input lengths, we propose to replace fully-connected layers in FFN with strided convolutions to progressively reduce the sequence length. The modified Transformer is dubbed strided Transformer encoder (STE), as shown in Fig. 1. Through the proposed STE, we can model both global and local information in a hierarchical architecture and it trades off the computation in FFN for constructing a deeper model to boost the model capacity.

One more question we address with our study is that, whether a single-pose representation is enough to represent a long sequence and how to make this representation work in improving the performance. We observe that directly supervising the model at a single target frame scale always breaks temporal smoothness between video frames, while only supervising at a full sequence scale cannot explicitly learn a specific representation for the target frame. These observations encourage us to develop a method that can effectively embed both scales into a learning-based framework. Therefore, based on the outputs of VTE and STE, a novel full-to-single supervision scheme is designed at both the full and single scales, which can enforce temporal smoothness and improve the representation ability of

features for the target frame.

The proposed architecture is called Strided Transformer, as shown in Figure 3. Extensive experiments are conducted on two standard 3D human pose estimation datasets, *i.e.*, Human3.6M [28] and HumanEva-I [29]. Experimental results show that the proposed method achieves state-of-the-art performance.

Our contributions are summarized as follows:

- We propose a new Transformer-based architecture for 3D human pose estimation, called Strided Transformer, which can simply and effectively lift 2D joint locations to 3D poses.
- To reduce the sequence redundancy and computation cost, strided Transformer encoder (STE) is introduced to progressively reduce the temporal dimensionality and aggregate long-range information to a single-vector representation of pose sequences in a hierarchical global and local fashion.
- A full-to-single supervision scheme is designed to impose extra temporal smoothness constraints during training at the full sequence scale and further refine the estimation at the single target frame scale.
- State-of-the-art results are achieved with fewer parameters on two commonly used benchmark datasets, making our method a strong baseline for Transformer-based 3D pose estimation.

## II. RELATED WORK

At the early stage of applying deep neural networks on 3D pose estimation task, many methods [30]–[33] learned the direct mapping from RGB images to 3D poses. However, these methods require sophisticated architectures with a high computation cost, which are impractical in realistic applications.

**Two-stage pose estimation.** Two-stage methods formulate the problem of 3D human pose estimation as 2D keypoint detection followed by 2D-3D lifting estimation [12], [34], [35]. Benefiting from the existing large-scale 2D pose datasets with sufficient annotations, this 2D-to-3D pose lifting method is widely used and achieves competitive performance. Martinez *et al.* [12] lifted 2D joint locations to 3D space via a fully-connected residual network. Fang *et al.* [34] proposed a pose grammar model to encode the human body configuration of human poses from 2D space to 3D space. We also follow this two-stage pipeline that is more popular among state-of-the-art methods in this domain.

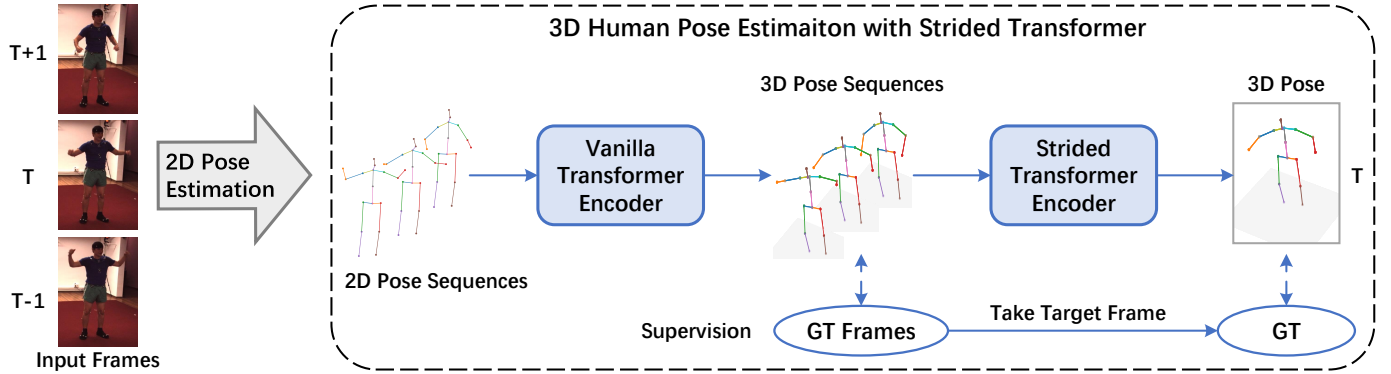


Fig. 3: Overview of our proposed Strided Transformer for predicting the 3D joint locations of the target frame from the estimated 2D pose sequences. It mainly consists of a vanilla Transformer encoder (VTE) and a strided Transformer encoder (STE) with a two-stage architecture design. The network first models long-range information via VTE and then aggregates the information to one target pose representation from the proposed STE. The model is trained end-to-end at both the full sequence scale and single target frame scale.

**Video pose estimation.** Since past and future frames are beneficial for 3D human pose estimation when the pose of a person is ambiguous or the body is partially occluded in one frame, many approaches tried to exploit temporal information [13], [16], [17], [36]. To predict temporally consistent 3D poses, Hossain *et al.* [16] designed a sequence-to-sequence network with LSTM. Pavlo *et al.* [13] introduced a fully convolutional model based on dilated temporal convolutions. Cai *et al.* [17] directly chose the 3D pose of the target frame from outputs of the proposed graph-based method and then fed it to a refinement model. To produce smoother 3D sequences, Wang *et al.* [36] designed an U-shaped graph convolutional network and involved motion modeling into learning. However, the temporal connectivity of these architectures is inherently limited and mainly constrained to simply sequential correlation. Different from most existing works that employed LSTM-based, graph-based, or fully convolutional architectures to exploit temporal information, we propose to leverage a Transformer-based architecture to capture long-range dependencies from input 2D pose sequences. Furthermore, compared to previous methods [17], [36] that either utilize a refinement model or use a motion loss, we design a full-to-single supervision scheme to produce predictions at both the full sequence scale and single target frame scale which further refines the intermediate predictions to produce more accurate estimations.

**Visual Transformers.** Transformer architecture was first proposed by [18] and commonly used in various language tasks. Recently, Transformer has shown promising performance in computer vision task, such as object detection [37], [38] and image classification [39], [40]. DETR [37] presented a new Transformer-based design for object detection systems. ViT [39] proposed to apply a standard Transformer architecture directly to sequential image patches for the basic image classification task. To reconstruct 3D human pose and mesh, Lin *et al.* [41] introduced a Transformer framework (METRO) from a single image. However, METRO focused on the one-stage estimation and ignored the temporal information across frames. Unlike DETR [37], ViT [39], and METRO

[41] that directly applied Transformer to images, we exploit Transformer to map 2D keypoints to 3D poses. Additionally, different from Zheng *et al.* [42] that applied a pure Transformer to model human joint relations and temporal correlations across frames, our method incorporates local contexts into the standard Transformer to deal with the redundancy of sequences for the video-based 3D pose estimation task.

### III. STRIDED TRANSFORMER

In this section, we first give an overview of the proposed framework for 3D human pose estimation from a 2D video stream, and then show how our Transformer-based architecture learns a representative single-pose representation from redundant sequences resulting in an enhanced estimation. Finally, the complexity analysis of our network is presented.

#### A. Overview

The overall framework of our proposed method is illustrated in Fig. 3. Given a sequence of the estimated 2D poses  $P = \{p_1, \dots, p_T\}$  from videos, we aim to reconstruct 3D joint locations  $X \in \mathbb{R}^{J \times 3}$  for a target frame (center frame), where  $p_t \in \mathbb{R}^{J \times 2}$  denotes the 2D joint locations at frame  $t$ ,  $T$  is the number of video frames, and  $J$  is the number of joints. The network contains a vanilla Transformer encoder (VTE) followed by a strided Transformer encoder (STE), which is trained in a full-to-single prediction scheme at both the full sequence scale and single target frame scale. Specifically, VTE is first used to model long-range information and is supervised by the full sequence scale to enforce temporal smoothness. Then, the proposed STE aggregates the information to one target pose representation and is supervised by the single target frame scale to produce more accurate estimations.

#### B. Strided Transformer Encoder

Despite the substantial performance gains achieved by the Transformer architecture [18] in many computer vision tasks, the full-length token-level representation makes it unsuitable

for many video-based vision tasks that only require a single-vector representation of the sequence. With this intuition, STE is proposed to gradually compress the sequence of hidden states to a shorter one and model both global and local information in a hierarchical architecture. Each layer of the proposed STE consists of a multi-head self-attention (MSA) and a convolutional feed-forward network (CFFN).

1) *Multi-head self-attention*: The core mechanism of Transformer is MSA [18]. Suppose there are a set of queries ( $Q$ ), keys ( $K$ ), and values ( $V$ ) of dimension  $d_m$ , then MSA can be computed as:

$$head_i = \text{Self-Attn} \left( QW_i^Q, KW_i^K, VW_i^V \right), \quad (1)$$

$$\text{MSA}(Q, K, V) = \text{Concat}(head_1, \dots, head_h) W^O, \quad (2)$$

where  $\text{Self-Attn}(Q, K, V) = \text{softmax} \left( QK^T / \sqrt{d_k} \right) V$  and  $W_i^Q \in \mathbb{R}^{d_m \times d_k}$ ,  $W_i^K \in \mathbb{R}^{d_m \times d_k}$ ,  $W_i^V \in \mathbb{R}^{d_m \times d_v}$ , and  $W^O \in \mathbb{R}^{hd_v \times d_m}$  are parameter matrices. The hyperparameter  $h$  is the number of multi-attention heads,  $d_m$  is the dimension of model, and  $d_k = d_v = d_m/h$  in our implementation.

2) *Convolutional feed-forward network*: In the existing fully connected (FC) layers in the FFN of VTE (Eq. (3)), it always maintains a full-length sequence of hidden representations across all layers with a high computation cost. It contains significant redundancy for video-based pose estimation, as nearby poses are quite similar. However, to reconstruct more accurate 3D body joints of the target frame, crucial information should be extracted from the entire pose sequences. Therefore, it requires selectively aggregating useful information.

To tackle this issue, inspired by the previous works [13], [27] that employ temporal convolutions to handle varying length sequences, we make modifications to the generic FFN. Given the input feature vector  $Z \in \mathbb{R}^{T \times D_{in}}$  with  $T$  sequences and  $D_{in}$  channels to generate an output of  $(\tilde{T}, D_{out})$  features, the operation performed by FC in FFN can be formulated as:

$$\text{FC}_{t,d_{out}}(z) = \sum_i^{D_{in}} w_{d_{out},i} * z_{t,i}. \quad (3)$$

If 1D convolution is considered with kernel size  $K$  and strided factor  $S$ , a strided convolution in CFFN can be computed as:

$$\text{Conv}_{S(t),c_{out}}(z) = \sum_i^{D_{in}} \sum_k^K w_{d_{out},i,k} * z_{S(t - \frac{K-1}{2} + k),i}. \quad (4)$$

3) *Network structure*: In this way, fully-connected layers in FFN of VTE are replaced with strided convolutions. The modified VTE is termed as strided Transformer encoder (STE), which consists of a MSA and a CFFN. Mathematically, it can be represented as:

$$\hat{Z}^{n-1} = Z^{n-1} + \text{MSA}(\text{LN}(Z^{n-1})), \quad (5)$$

$$Z^n = \text{MaxPool}(\hat{Z}^{n-1}) + \text{CFFN}(\text{LN}(\hat{Z}^{n-1})), \quad (6)$$

where  $\text{LN}(\cdot)$  denotes the layer normalization operation,  $\text{MaxPool}(\cdot)$  denotes the max pooling operation, and  $n \in [1, \dots, N]$  is the index of layers.

STE is a hierarchical global and local architecture, where self-attention mechanism models global context and strided

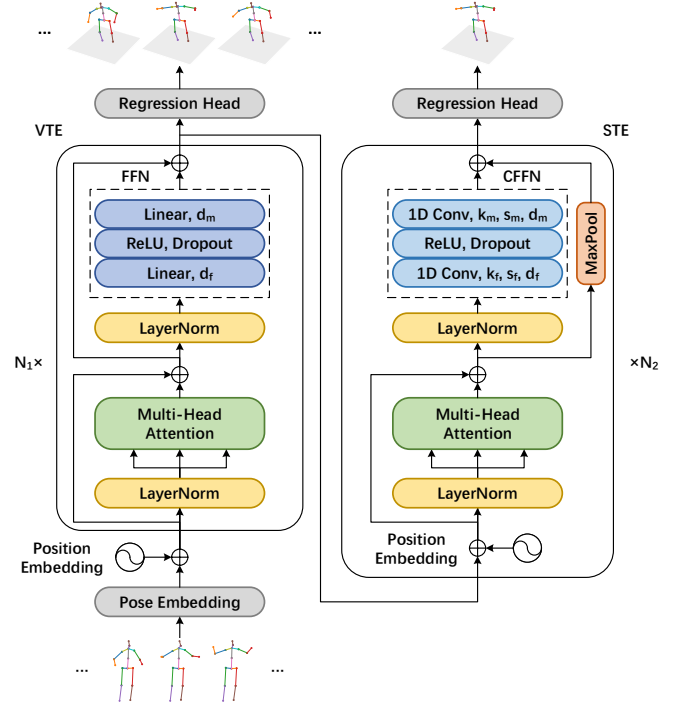


Fig. 4: The network architecture of our proposed Strided Transformer, where the left is VTE and the right is STE with strided convolutions. Here,  $N_1$  and  $N_2$  denote the layers of the two modules, respectively. The hyperparameters  $k$ ,  $s$ ,  $d_m$  and  $d_f$  are the kernel size, the strided factor, the dimensions, and the number of hidden units. The max pooling operation is applied to the residuals to match the temporal dimensions.

convolution helps capture local context, as presented in Fig. 4 (right). It gradually shrinks the sequence length from layer to layer and merges the nearby poses to a short sequence length representation, illustrated in Fig. 5. More importantly, from such a hierarchical design, the redundancy of all frames and the computation cost is reduced.

### C. 3D Pose Estimation with Strided Transformer

In this section, we describe how to use the proposed Transformer-based architecture to estimate 3D human poses with a sequence of 2D poses. As shown in Fig. 5, the proposed network is composed of four components: a pose embedding, a vanilla Transformer encoder, a strided Transformer encoder, and a regression head.

1) *Pose embedding*: Given a sequence of the estimated 2D poses  $P \in \mathbb{R}^{T \times J \times 2}$ , the pose embedding first concatenates  $(x, y)$  coordinates of the  $J$  joints for each frame to tokens  $P' \in \mathbb{R}^{T \times (J \cdot 2)}$ , and then embeds each token to a high dimensional feature  $Z_0 \in \mathbb{R}^{T \times d_m}$  using a 1D convolutional layer with  $d_m$  channels, followed by batch normalization, dropout and a ReLU activation.

2) *Vanilla Transformer encoder*: Suppose that the VTE consists of  $N_1$  layers, the learnable position embedding  $E_1 \in \mathbb{R}^{T \times d_m}$  is used before the first layer of VTE, which can be formulated as follows:

$$Z_1^0 = Z_0 + E_1. \quad (7)$$



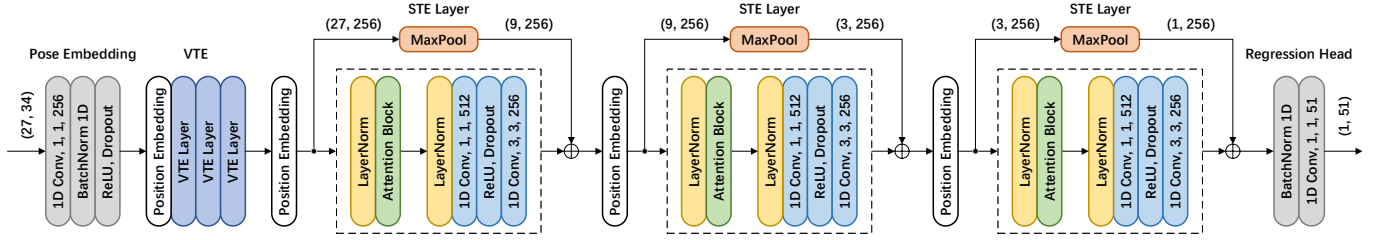


Fig. 5: An instantiation of the proposed Strided Transformer network, which reconstructs the target 3D body joints by progressively reducing the sequence length. The input consists of 2D keypoints for a receptive field of 27 frames with  $J = 17$  joints. Convolutional feed-forward networks are in blue where  $(3, 3, 256)$  denotes kernels of size 3 with strided factor 3, and 256 output channels. The tensor sizes are shown in parentheses, e.g.,  $(27, 34)$  denotes 27 frames and 34 channels. Due to strided convolutions, the max pooling operation is used to the residuals to match the shape of subsequent tensors.

Then, given the embedded feature  $Z_1^0$ , the VTE layers can be represented as:

$$\hat{Z}_1^{n-1} = Z_1^{n-1} + \text{MSA}(\text{LN}(Z_1^{n-1})), \quad (8)$$

$$Z_1^n = \hat{Z}_1^{n-1} + \text{FFN}(\text{LN}(\hat{Z}_1^{n-1})), \quad (9)$$

where  $n \in [1, \dots, N_1]$  is the index of VTE layers. It can be expressed by using a function of a VTE layer  $\text{VTE}(\cdot)$ :

$$Z_1^n = \text{VTE}(Z_1^{n-1}). \quad (10)$$

3) *Strided Transformer encoder*: For the STE, it is built upon the outputs of VTE and takes the  $Z_1^{N_1} \in \mathbb{R}^{T \times d_m}$  as input. The learnable position embeddings  $E_2 \in \mathbb{R}^{S(t) \times d_m}$  with strided factor  $S$  are used for the every layer of STE due to the different sequence lengths. Then, the STE layers can be represented as follows:

$$Z_2^n = \text{STE}(Z_2^{n-1} + E_2^n), \quad (11)$$

where  $n \in [1, \dots, N_2]$  is the index of STE layers,  $Z_2^0 = Z_1^{N_1}$ , and  $\text{STE}(\cdot)$  denotes the function of a STE layer whose details can be found in Eq. (5) and Eq. (6).

4) *Regression head*: In order to perform regression, a batch normalization and a 1D convolutional layer are applied to the outputs of VTE and STE modules,  $Z_1^{N_1} \in \mathbb{R}^{T \times d_m}$  and  $Z_2^{N_2} \in \mathbb{R}^{T \times d_m}$ , respectively. Finally, the outputs of 3D pose prediction are  $\tilde{X}$  and  $X$ , where  $\tilde{X} \in \mathbb{R}^{T \times J \times 3}$  and  $X \in \mathbb{R}^{J \times 3}$  are predictions of 3D pose sequences and target frame's 3D joint locations, respectively.

#### D. Transformer-based Full-to-Single Prediction

The iterative refinement scheme aimed at producing predictions in multiple processing stages is effective for 3D pose estimation [17], [30]. Inspired by the success of such iterative processing, we also consider a refinement scheme. Furthermore, to incorporate both full sequence scale and single target frame scale constraints into the framework, a full-to-single scheme is proposed, which further refines the intermediate predictions to produce more accurate estimations rather than using a single component with a single output. More precisely, the full sequence scale can enforce temporal smoothness and the single target frame scale helps learn a specific representation for the target frame.

1) *Full sequence scale*: The first step is to supervise with full sequence scale by imposing extra temporal smoothness constraints during training from the output of VTE followed by a regression head. A sequence loss  $\mathcal{L}_f$  is adopted to improve upon single frame predictions for temporal consistency over a sequence. This loss ensures that the estimated 3D pose sequences  $\tilde{X} \in \mathbb{R}^{T \times J \times 3}$  coincide with the ground-truth 3D joint sequences  $Y \in \mathbb{R}^{T \times J \times 3}$ :

$$\mathcal{L}_f = \sum_{t=1}^T \sum_{i=1}^J \|Y_i^t - \tilde{X}_i^t\|_2, \quad (12)$$

where  $\tilde{X}_i^t$  and  $Y_i^t$  represent the sequence of estimated 3D poses and ground truth 3D joint locations of joint  $i$  at frame  $t$ , respectively.

2) *Single target frame scale*: In the second step, the supervision is upon the output of STE, which is a progressive reduction architecture to reduce the temporal dimensionality from layer to layer, followed by a regression head. The output is a prediction of the target frame's 3D joint locations from the input sequences using both past and future data. A single-frame loss  $\mathcal{L}_s$  is used to minimize the distance between the estimated 3D pose  $X \in \mathbb{R}^{J \times 3}$  and the target ground-truth 3D joint annotation  $Y \in \mathbb{R}^{J \times 3}$ :

$$\mathcal{L}_s = \sum_{i=1}^J \|Y_i - X_i\|_2, \quad (13)$$

where  $X_i$  and  $Y_i$  represent the target frame's estimated 3D pose and ground truth 3D joint locations of joint  $i$ , respectively.

3) *Loss function*: In our implementation, the model is supervised at both the full sequence scale and single target frame scale. The entire network is trained in an end-to-end manner with the combined loss:

$$\mathcal{L} = \lambda_f \mathcal{L}_f + \lambda_s \mathcal{L}_s, \quad (14)$$

where  $\lambda_f$  and  $\lambda_s$  are weighting factors.

#### E. Complexity Analysis

In this section, floating-point operations (FLOPs) is used to measure the computational cost and analyze the compression ratio of our proposed Strided Transformer network. Given the

sequences length  $t$ , dimensions  $d_m = d_f/2 = d$ , a fixed strided factor  $s$ , and a kernel size  $k$ , the FLOPs of a VTE layer  $\mathcal{F}_{VTE}^n$  and a STE layer  $\mathcal{F}_{STE}^n$  can be computed by:

$$\begin{aligned}\mathcal{F}_{VTE}^n(t, d) &= \mathcal{F}_{MSA}^n(t, d) + \mathcal{F}_{FFN}^n(t, d) \\ &= 8td^2 + 2t^2d,\end{aligned}\quad (15)$$

$$\begin{aligned}\mathcal{F}_{STE}^n(t, d, s) &= \mathcal{F}_{MSA}^n(t, d, s) + \mathcal{F}_{CFN}^n(t, d, s) \\ &= (6 + 2s^{-1}k)td^2 + 2t^2d,\end{aligned}\quad (16)$$

where  $\mathcal{F}_{MSA}^n$ ,  $\mathcal{F}_{FFN}^n$  and  $\mathcal{F}_{CFN}^n$  are the FLOPs of the MSA, FFN and CFN, respectively.

Then if we consider  $N$  layers of VTE and STE with input sequence length  $T$ , dimensions  $D$ , strided factor  $S$ , and kernel size  $K$ , the encoder-wise FLOPs of VTE  $\mathcal{F}_{VTE}$  can be formulated as:

$$\mathcal{F}_{VTE} = N\mathcal{F}_{VTE}^n = N(8TD^2 + 2T^2D), \quad (17)$$

the encoder-wise FLOPs of STE  $\mathcal{F}_{STE}$  can be formulated as:

$$\begin{aligned}\mathcal{F}_{STE} &= \sum_{n=1}^N \mathcal{F}_{STE}^n \\ &= \sum_{n=1}^N \left[ \left( \frac{6 + 2KS^{-1}}{S^{n-1}} \right) TD^2 + \frac{2}{S^{2(n-1)}} T^2D \right] \\ &= \frac{(6S + 2K)(1 - S^{-N})}{S - 1} TD^2 + \frac{2S^2(1 - S^{-2N})}{S^2 - 1} T^2D.\end{aligned}\quad (18)$$

For our 27-frame Strided Transformer, which contains  $N_1$  VTE layers and  $N_2$  STE layers with  $N_1 = N_2 = N = 3$ ,  $S = 3$ , and  $K = 3$ . In this case, the compression ratio  $\alpha$  can be computed by:

$$\begin{aligned}\alpha &= \frac{2\mathcal{F}_{VTE}}{\mathcal{F}} = (2N\mathcal{F}_{VTE}^n) / \left( N\mathcal{F}_{VTE}^n + \sum_{n=1}^N \mathcal{F}_{STE}^n \right) \\ &= \frac{2}{1 + \beta},\end{aligned}\quad (19)$$

where

$$\beta = \frac{\mathcal{F}_{STE}}{\mathcal{F}_{VTE}} = \frac{468D + 91T}{972D + 243T}. \quad (20)$$

We have  $\lim_{D \rightarrow \infty} \alpha = 1.35$  with a fixed  $T$ , which indicates the compression ratio  $\alpha$  of our 27-frame Strided Transformer is 1.35.

## IV. EXPERIMENTS

### A. Datasets and Evaluation

The proposed method is evaluated on two challenging benchmark datasets, *i.e.*, Human3.6M [28] and HumanEva-I [29]. The Human3.6M dataset is the largest publicly available dataset for 3D human pose estimation, which consists of 3.6 million images captured from 4 synchronized 50 Hz cameras. There are 7 professional subjects performing 15 everyday activities such as “Waiting”, “Smoking”, and “Posing”. Following the standard protocol in prior works [13], [50], [51], 5 subjects (S1, S5, S6, S7, S8) are used for training and 2 subjects (S9 and S11) are used for evaluation. The frames from all views are trained by a single model for all actions.

HumanEva-I is a much smaller dataset with fewer subjects and actions compared to Human3.6M. Following [13], [15], a single model is trained for all subjects (S1, S2, S3) and all actions (Walk, Jog, Box).

Three standard evaluation protocols are used in the experiments. The mean per joint position error (MPJPE) is the average Euclidean distance between the ground-truth and predicted positions of the joints, which is referred to as protocol #1 in many works [34], [52]. Procrustes analysis MPJPE (P-MPJPE) is adopted, where the estimated 3D pose is aligned to the ground truth in translation, rotation, and scale, which is referred to as protocol #2 [12], [16]. Following [13], [36], [47], we also report the mean per joint velocity error (MPJVE) corresponding to the MPJPE of the first derivative of the 3D pose sequences. This metric measures the smoothness of predicted over time, which is important for video.

### B. Implementation Details

In our experiments, the proposed Strided Transformer contains encoder layers  $N_1 = N_2 = 3$ , multi-attention heads  $h = 8$ , dimensions  $d_m = 256$ , and hidden units  $d_f = 512$  for both VTE and STE. The kernel sizes  $k_f$  is set to 1 and  $k_m$  is set to 3 in all STE layers. The strided factor  $s_f$  is set to 1, and  $s_m$  is set to  $\{3, 3, 3\}$  for the receptive field of 27 frames,  $\{3, 3, 9\}$  for 81,  $\{3, 9, 9\}$  for 243, and  $\{3, 9, 13\}$  for 351. The weighting factors  $\lambda_f$  and  $\lambda_s$  are set to 1.

All experiments are conducted on the PyTorch framework with one GeForce GTX 3090 GPU. The network is trained using the Adam optimizer with a mini-batch size of 256 for Human3.6M and 64 for HumanEva-I. An initial learning rate of 0.001 is used with a shrink factor of 0.95 applied after each epoch and 0.5 after every 5 epochs. The same refine module as [17], [36] is adopted. Note that we only apply horizontal flip augmentation during training and test stages and only compute MPJPE loss for training.

The 2D poses can be obtained by performing any classic 2D pose detections or directly using the 2D ground truth. Following [13], [53], the cascaded pyramid network (CPN) [54] is used for Human3.6M and Mask R-CNN [55] is adopted for HumanEva-I to obtain 2D poses for a fair comparison.

### C. Comparison with State-of-the-art Results

Our method is compared with previous state-of-the-art approaches on Human3.6M dataset. As shown in Table I, the performance of our 351-frame model with CPN input is presented. Our method outperforms the state-of-the-art methods on Human3.6 under all metrics (43.6 mm on protocol #1 and 34.9 mm on protocol #2).

Table II compares the MPJPE metric and number of parameters with several state-of-the-art methods in different receptive fields on Human3.6M. It can be seen that our method has the fewest parameters but achieves the best performance. This shows that our proposed Transformer-based network is more efficient than fully convolutional architectures [13], [27], [47] at the same level of accuracy for 3D pose estimation in videos. Besides, our model is lightweight and parameters hardly increase with the increased receptive fields, which is practical for

TABLE I: Quantitative comparisons with the state-of-the-art methods on Human3.6M under protocol #1 and protocol #2, where † indicates that the input 2D pose is detected by cascaded pyramid network (CPN). Best in bold, second-best underlined.

Protocol #1	Dir.	Disc	Eat	Greet	Phone	Photo	Pose	Purch.	Sit	SitD.	Smoke	Wait	WalkD.	Walk	WalkT.	Avg.
Martinez <i>et al.</i> [12] ICCV'17	51.8	56.2	58.1	59.0	69.5	78.4	55.2	58.1	74.0	94.6	62.3	59.1	65.1	49.5	52.4	62.9
Fang <i>et al.</i> [34] AAAI'18	50.1	54.3	57.0	57.1	66.6	73.3	53.4	55.7	72.8	88.6	60.3	57.7	62.7	47.5	50.6	60.4
Xu <i>et al.</i> [35] CVPR'21 †	45.2	49.9	47.5	50.9	54.9	66.1	48.5	46.3	59.7	71.5	51.4	48.6	53.9	39.9	44.1	51.9
Gong <i>et al.</i> [43] CVPR'21	-	-	-	-	-	-	-	-	-	-	-	-	-	-	-	50.2
Cai <i>et al.</i> [17] ICCV'19 †	44.6	47.4	45.6	48.8	50.8	59.0	47.2	43.9	57.9	61.9	49.7	46.6	51.3	37.1	39.4	48.8
Pavlo <i>et al.</i> [13] CVPR'19 †	45.2	46.7	43.3	45.6	48.1	55.1	44.6	44.3	57.3	65.8	47.1	44.0	49.0	32.8	33.9	46.8
Lin <i>et al.</i> [44] BMVC'19 †	42.5	44.8	42.6	44.2	48.5	57.1	42.6	41.4	56.5	64.5	47.4	43.0	48.1	33.0	35.1	46.6
Xu <i>et al.</i> [45] CVPR'20 †	<b>37.4</b>	43.5	42.7	42.7	46.6	59.7	<b>41.3</b>	45.1	<b>52.7</b>	60.2	45.8	43.1	47.7	33.7	37.1	45.6
Liu <i>et al.</i> [27] CVPR'20 †	41.8	44.8	41.1	44.9	47.4	54.1	43.4	42.2	56.2	63.6	<u>45.3</u>	43.5	45.3	<u>31.3</u>	32.2	45.1
Zeng <i>et al.</i> [46] ECCV'20 †	46.6	47.1	43.9	41.6	<b>45.8</b>	<b>49.6</b>	46.5	<u>40.0</u>	<u>53.4</u>	61.1	46.1	42.6	<b>43.1</b>	31.5	32.6	44.8
Wang <i>et al.</i> [36] ECCV'20 †	40.2	<b>42.5</b>	42.6	<u>41.1</u>	46.7	56.7	41.4	42.3	56.2	<u>60.4</u>	46.3	<u>42.2</u>	46.2	31.7	<u>31.0</u>	44.5
Chen <i>et al.</i> [47] TCSVT'21 †	41.4	43.5	<u>40.1</u>	42.9	46.6	51.9	41.7	42.3	53.9	<b>60.2</b>	45.4	<b>41.7</b>	46.0	31.5	32.7	<u>44.1</u>
Ours †	<u>39.9</u>	<u>43.4</u>	<b>40.0</b>	<b>40.9</b>	<u>46.4</u>	<u>50.6</u>	42.1	<b>39.8</b>	55.8	61.6	<b>44.9</b>	43.3	<u>44.9</u>	<b>29.9</b>	<b>30.3</b>	<b>43.6</b>
Protocol #2	Dir.	Disc	Eat	Greet	Phone	Photo	Pose	Purch.	Sit	SitD.	Smoke	Wait	WalkD.	Walk	WalkT.	Avg.
Martinez <i>et al.</i> [12] ICCV'17	39.5	43.2	46.4	47.0	51.0	56.0	41.4	40.6	56.5	69.4	49.2	45.0	49.5	38.0	43.1	47.7
Pavlakos <i>et al.</i> [48] CVPR'18	34.7	39.8	41.8	38.6	42.5	47.5	38.0	36.6	50.7	56.8	42.6	39.6	43.9	32.1	36.5	41.8
Liu <i>et al.</i> [49] ECCV'20 †	35.9	40.0	38.0	41.5	42.5	51.4	37.8	36.0	48.6	56.6	41.8	38.3	42.7	31.7	36.2	41.2
Gong <i>et al.</i> [43] CVPR'21	-	-	-	-	-	-	-	-	-	-	-	-	-	-	-	39.1
Cai <i>et al.</i> [17] ICCV'19 †	35.7	37.8	36.9	40.7	39.6	45.2	37.4	34.5	46.9	50.1	40.5	36.1	41.0	29.6	33.2	39.0
Pavlo <i>et al.</i> [13] CVPR'19 †	34.1	36.1	34.4	37.2	36.4	42.2	34.4	33.6	<u>45.0</u>	52.5	37.4	33.8	37.8	25.6	27.3	36.5
Xu <i>et al.</i> [45] CVPR'20 †	<b>31.0</b>	<b>34.8</b>	34.7	34.4	<u>36.2</u>	43.9	31.6	33.5	<b>42.3</b>	49.0	37.1	33.0	39.1	26.9	31.9	36.2
Liu <i>et al.</i> [27] CVPR'20 †	32.3	35.2	33.3	35.8	35.9	41.5	33.2	32.7	44.6	50.9	37.0	32.4	37.0	25.2	27.2	35.6
Wang <i>et al.</i> [36] ECCV'20 †	32.9	35.2	35.6	<b>34.4</b>	36.4	42.7	<b>31.2</b>	32.5	45.6	50.2	37.3	<u>32.8</u>	36.3	26.0	<b>23.9</b>	35.5
Chen <i>et al.</i> [47] TCSVT'21 †	32.6	<u>35.1</u>	<u>32.8</u>	35.4	36.3	<b>40.4</b>	32.4	<u>32.3</u>	<u>42.7</u>	<u>49.0</u>	<u>36.8</u>	<b>32.4</b>	<u>36.0</u>	<u>24.9</u>	26.5	<u>35.0</u>
Ours †	<u>32.0</u>	35.6	<b>32.6</b>	<u>35.1</u>	<b>35.8</b>	<u>40.9</u>	33.2	<b>31.2</b>	44.7	<b>48.9</b>	<b>36.7</b>	33.9	<b>35.2</b>	<b>23.7</b>	<u>25.1</u>	<b>34.9</b>

TABLE II: Quantitative comparisons with state-of-the-art methods in different receptive fields on Human3.6M. The MPJPE metric and number of parameters are reported. The input 2D pose is detected by CPN.

Model	$T$	Param (M)	MPJPE (mm)
Pavlo <i>et al.</i> [13]	27	8.56	48.8
Pavlo <i>et al.</i> [13]	81	12.75	47.7
Pavlo <i>et al.</i> [13]	243	16.95	46.8
Liu <i>et al.</i> [27]	27	5.69	48.5
Liu <i>et al.</i> [27]	81	8.46	46.3
Liu <i>et al.</i> [27]	243	11.25	45.1
Chen <i>et al.</i> [47]	27	31.88	45.3
Chen <i>et al.</i> [47]	81	45.53	44.6
Chen <i>et al.</i> [47]	243	59.18	44.1
Ours (27 frames)	27	4.01	46.9
Ours (81 frames)	81	4.06	45.4
Ours (243 frames)	243	4.23	44.0
Ours (351 frames)	351	4.34	<b>43.6</b>

real-time applications. Fig. 7 shows the visualized qualitative results from 243-frame models of TCN [13], ATTN-TCN [27], and our model.

Additionally, the results are reported when using ground truth 2D poses to explore the upper bound of our method. As illustrated in Table III, it can be seen that our method achieves the best result (28.6 mm in MPJPE) outperforming all other methods. Moreover, it has a larger performance gain than CPN input compared with state-of-the-art methods, which indicates that our method has a stronger capacity in capturing temporal dependencies from more accurate 2D representations.

As shown in Table IV, with the supervision of full sequence scale, our method reduces the MPJVE by 19.2% (from 2.6 mm to 2.1 mm) achieving more smooth predictions with lower MPJVE than other models. This indicates the full-to-single supervision scheme can enforce temporal smoothness

and produce vastly smoother poses.

To evaluate the generalizability of our model to smaller datasets, experiments are conducted on HumanEva-I based on Mask R-CNN 2D detections and 2D ground truth. The results are given in Table V, which demonstrates that our method achieves promising results in each action.

#### D. Ablation Studies

**Input sequence length.** The MPJPE results of our model with different sequence lengths (between 1 and 351) on Human3.6M are shown in Fig. 6 (a). It can be seen that with more input frames used for predictions, our proposed method obtains larger gains under both 2D pose inputs (CPN and GT), but the error saturates past a certain point. This is expected since directly lifting 3D poses from disjointed 2D poses leads to temporally incoherent outputs [56]. It is worth mentioning that our method get the better result with  $T = 351$  (43.6 mm) than  $T = 243$  (44.0 mm), while the performance decreases with longer inputs ( $T > 243$ ) in [27]. This indicates that our method equipped with global self-attention mechanism shows great power in modeling long-range dependencies. More importantly, with the help of STE, our method can distinguish the representative representation from redundant long sequences. Next, we choose  $T = 27$  on Human3.6M in the following ablation experiments as a compromise between the accuracy and the computational complexity.

**2D detections.** For the 2D-3D lifting task, the accuracy of the 2D detections directly influences the results of 3D pose estimation [12]. To show the effectiveness of our method on different 2D pose detectors, we carry out experiments with the detections from Stack Hourglass (SH) [57], Detectron [13], and CPN [54]. Moreover, to test the tolerance of our method to different levels of noise, we also train our network by 2D

TABLE III: Quantitative comparisons of MPJPE in millimeter on Human3.6M under protocol #1, using ground truth 2D joint locations as input. Best in bold.

Protocol #1	Dir.	Disc	Eat	Greet	Phone	Photo	Pose	Purch.	Sit	SitD.	Smoke	Wait	WalkD.	Walk	WalkT.	Avg.
Martinez <i>et al.</i> [12] ICCV'17	37.7	44.4	40.3	42.1	48.2	54.9	44.4	42.1	54.6	58.0	45.1	46.4	47.6	36.4	40.4	45.5
Lee <i>et al.</i> [15] ECCV'18	32.1	36.6	34.3	37.8	44.5	49.9	40.9	36.2	44.1	45.6	35.3	35.9	30.3	37.6	35.5	38.4
Pavlo <i>et al.</i> [13] CVPR'19	35.2	40.2	32.7	35.7	38.2	45.5	40.6	36.1	48.8	47.3	37.8	39.7	38.7	27.8	29.5	37.8
Cai <i>et al.</i> [17] ICCV'19	32.9	38.7	32.9	37.0	37.3	44.8	38.7	36.1	41.0	45.6	36.8	37.7	37.7	29.5	31.6	37.2
Xu <i>et al.</i> [35] CVPR'21	35.8	38.1	31.0	35.3	35.8	43.2	37.3	31.7	38.4	45.5	35.4	36.7	36.8	27.9	30.7	35.8
Liu <i>et al.</i> [27] CVPR'20	34.5	37.1	33.6	34.2	32.9	37.1	39.6	35.8	40.7	41.4	33.0	33.8	33.0	26.6	26.9	34.7
Chen <i>et al.</i> [47] TCSVT'21	-	-	-	-	-	-	-	-	-	-	-	-	-	-	-	32.3
Zeng <i>et al.</i> [46] ECCV'20	34.8	32.1	28.5	30.7	31.4	36.9	35.6	30.5	38.9	40.5	32.5	31.0	29.9	22.5	24.5	32.0
Ours	<b>27.9</b>	<b>29.9</b>	<b>26.8</b>	<b>27.8</b>	<b>28.6</b>	<b>32.8</b>	<b>31.1</b>	<b>26.7</b>	<b>36.5</b>	<b>35.5</b>	<b>30.0</b>	<b>29.8</b>	<b>27.5</b>	<b>19.6</b>	<b>19.7</b>	<b>28.6</b>

TABLE IV: Results show the velocity error (MPJPV) of our methods and other state-of-the-arts on Human3.6M. Here, \* denotes that our result without the supervision of full sequence scale. Best in bold.

MPJPV	Dir.	Disc	Eat	Greet	Phone	Photo	Pose	Purch.	Sit	SitD.	Smoke	Wait	WalkD.	Walk	WalkT.	Avg.
Pavlo <i>et al.</i> [13] CVPR'19	3.0	3.1	2.2	3.4	2.3	2.7	2.7	3.1	2.1	2.9	2.3	2.4	3.7	3.1	2.8	2.8
Lin <i>et al.</i> [44] BMVC'19	2.7	2.8	2.1	3.1	2.0	2.5	2.5	2.9	1.8	2.6	2.1	2.3	3.7	2.7	3.1	2.7
Chen <i>et al.</i> [47] TCSVT'21	2.7	2.8	2.0	3.1	2.0	2.4	2.4	2.8	1.8	2.4	2.0	2.1	3.4	2.7	2.4	2.5
Wang <i>et al.</i> [36] ECCV'20	2.3	2.5	2.0	<b>2.7</b>	2.0	2.3	2.2	2.5	1.8	2.7	1.9	2.0	<b>3.1</b>	<b>2.2</b>	2.5	2.3
Ours *	2.8	2.8	2.1	3.2	2.2	2.5	2.6	2.8	1.8	2.4	2.1	2.3	3.5	3.0	2.6	2.6
Ours	<b>2.3</b>	<b>2.4</b>	<b>1.8</b>	2.8	<b>1.7</b>	<b>2.2</b>	<b>2.2</b>	<b>2.5</b>	<b>1.4</b>	<b>2.0</b>	<b>1.7</b>	<b>1.9</b>	3.2	2.6	<b>2.1</b>	<b>2.1</b>

TABLE V: Quantitative results on HumanEva-I dataset under protocol #2. Best in bold, second-best underlined. (MRCNN) - Mask-RCNN; (GT) - 2D ground truth.

	Walk			Jog			Box			Avg.
	S1	S2	S3	S1	S2	S3	S1	S2	S3	
Martinez <i>et al.</i> [12]	19.7	17.4	46.8	26.9	18.2	18.6	-	-	-	-
Pavlakos <i>et al.</i> [30]	22.3	19.5	<b>29.7</b>	28.9	21.9	23.8	-	-	-	-
Lee <i>et al.</i> [15]	18.6	19.9	<u>30.5</u>	25.7	16.8	17.7	42.8	48.1	53.4	30.3
Pavlo <i>et al.</i> [13]	<b>13.9</b>	<u>10.2</u>	46.6	<u>20.9</u>	<b>13.1</b>	<b>13.8</b>	<u>23.8</u>	<u>33.7</u>	<u>32.0</u>	<u>23.1</u>
Ours ( $T = 27$ MRCNN)	<u>14.0</u>	<b>10.0</b>	32.8	<b>19.5</b>	<u>13.6</u>	<u>14.2</u>	<b>22.4</b>	<b>21.6</b>	<b>22.5</b>	<b>18.9</b>
Ours ( $T = 27$ GT)	9.7	7.6	15.8	12.3	9.4	11.2	14.8	12.9	16.5	12.2

ground truth (GT) with different levels of additive Gaussian noises. The results are shown in Fig. 6 (b). It can be observed that the MPJPE of 3D poses increases linearly with the two-norm errors of 2D poses. Note that 2D pose detector methods achieve worse estimation performance than 2D ground truth with noises, which is due to the self-occlusions problem for 2D pose estimation.

**Model hyperparameters.** As shown in Table VI, we first analyze the effect of the number of VTE layers. Empirically, it can be found that the performance cannot be improved when naively stacking multiple standard Transformer encoder layers. However, our model that introduces STE is more accurate at the same level of the number of Transformer encoder layers and comparable model parameters. For example, our method ( $N_1 = 3$  and  $N_2 = 3$ ) has better performance and fewer FLOPs than  $N_1 = 6$  at the same  $d_m = 256$  and  $d_f = 512$  hidden units (46.9 mm vs. 47.9 mm, 128.88M vs. 174.36M). In addition, our STE ( $N_2 = 3$ , 41.72M) also has fewer FLOPs than standard Transformer encoder ( $N_1 = 3$ , 87.16M) with similar parameters, which achieves  $2.1\times$  less computation. It verifies the effectiveness of our proposed STE that reduces the redundancy of the sequence and computation cost. Then, we investigate the hyperparameters on the performance and

parameters of both modules. It can be observed that using 3 encoder layers, 256 dimensions, and 512 hidden units achieves the best performance.

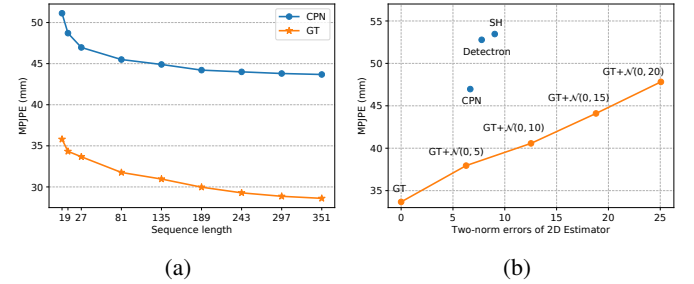


Fig. 6: (a) Ablation studies on different sequence lengths of our method on Human3.6M with the MPJPE metric. (b) The impact of 2D detections on Human3.6M. Here,  $\mathcal{N}(0, \sigma^2)$  represents the Gaussian noise with mean zero and  $\sigma$  is the standard deviation. (CPN) - Cascaded Pyramid Network; (SH) Stack Hourglass; (GT) - 2D ground truth.

**Strided factor.** The design choice of strided factor for STE is explored when fixing VTE with 3 encoder layers and 8 multi-attention heads, 256 dimensions, and 512 hidden units for both VTE and STE. The experimental results have been depicted in Table VII. It shows that using a strided factor  $s_m = \{3, 3, 3\}$  has the best performance. This demonstrates the benefit of leveraging a progressive reduction architecture to gradually reduce the temporal dimensionality from layer to layer with a small strided factor.

**Prediction scheme.** We further examine the proposed prediction scheme of full sequence scale and single target frame scale by using five different designs: (i) Full: the STE of our proposed method is replaced with VTE, and the new architecture is only supervised by the full sequence scale (the sequence loss). (ii) Single: the proposed method is only supervised by the single target frame scale (single-frame loss). (iii) Full-



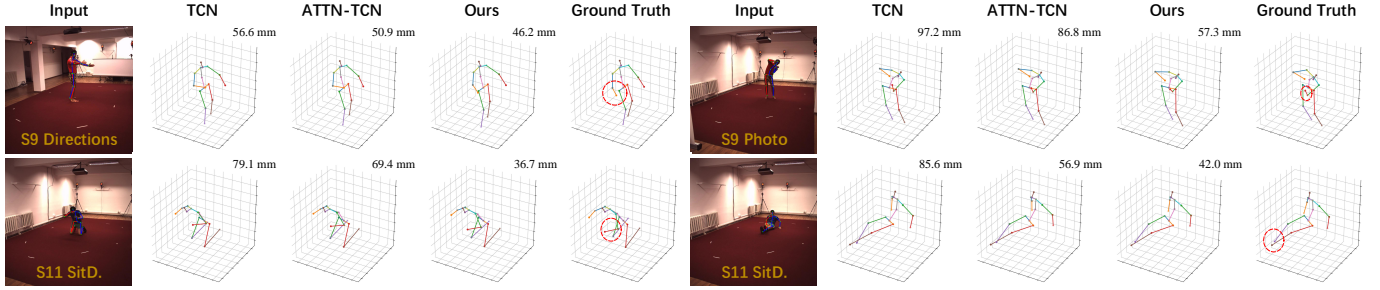


Fig. 7: Qualitative comparisons with the previous state-of-the-art methods, 243-frame model of TCN [13] and ATTN-TCN [27] on Human3.6M dataset.

TABLE VI: Ablation study on the hyperparameters of our model on Human3.6M under protocol #1.  $N_1$  and  $N_2$  are the number of VTE and STE layers, respectively.  $d_m$  and  $d_f$  are the dimensions and the number of hidden units.

$N_1$	$N_2$	$d_m$	$d_f$	Param (M)	FLOPs (M)	MPJPE (mm)
2	-	512	2048	6.36	342.74	47.9
3	-	512	2048	9.51	514.08	47.8
4	-	512	2048	12.66	685.44	48.0
5	-	512	2048	15.82	856.82	48.4
6	-	512	2048	18.97	1028.18	49.3
<hr/>						
2	-	256	512	1.08	58.12	47.8
3	-	256	512	1.61	87.16	47.6
4	-	256	512	2.13	116.22	47.8
5	-	256	512	2.66	145.30	47.7
6	-	256	512	3.19	174.36	47.9
<hr/>						
-	3	256	512	2.42	41.72	48.0
2	3	256	512	3.48	99.84	47.4
3	3	256	512	4.01	128.88	<b>46.9</b>
2	3	512	2048	22.18	589.78	47.4
3	3	512	2048	25.33	761.12	47.3

TABLE VII: Ablation study on the strided factor of STE with the receptive field  $T = 3 \times 3 \times 3 = 27$ . The evaluation is performed on Human3.6M under protocol #1.

Layers	Strided factor	MPJPE (mm)
3	3, 3, 3	<b>46.9</b>
3	3, 9, 1	47.5
3	9, 3, 1	47.3
2	3, 9	47.2
2	9, 3	47.1
1	27	47.7

to-full: the architecture consists of six layers VTE, whose first three layers and final three layers are both supervised by the sequence loss. (iv) Single-to-single: VTE and STE of the proposed method are both supervised by the single-frame loss. (v) Full-to-single: our proposed method. In Table VIII, it can be observed that the schemes of considering only one prediction manner (i, ii, iii, iv) decay performance, and our full-to-single prediction scheme (v) is best. The empirical results indicate that our proposed full-to-single mechanism at both the full and single scales can improve the representation ability of features and use further processing to produce more accurate predictions.

**Model components.** As shown in Table IX, an ablation

TABLE VIII: Ablation study on different prediction schemes. The evaluation is performed on Human3.6M under protocol #1.  $\Delta$  represents the performance gap between the methods and our proposed.

Prediction scheme	MPJPE (mm)	$\Delta$
Full	47.9	1.0
Single	48.3	1.4
Full-to-full	47.4	0.5
Single-to-single	48.5	1.6
Full-to-single	<b>46.9</b>	-

TABLE IX: Ablation study on each component of our network architecture on Human3.6M under protocol #1.

Method	MPJPE (mm)
Ours, proposed	<b>46.9</b>
Ours, intermediate predictions	48.1
Ours, Pooling Transformer	47.3
<hr/>	
w/o VTE	48.0
w/o STE	47.6

study is performed to assess the effectiveness of different components of our method. We select the center frame of intermediate predictions from VTE as final results, the MPJPE increases by 1.2 mm (from 46.9 mm to 48.1 mm). This proves that the intermediate supervision allows for a stronger capacity in producing more accurate 3D sequences. Following [20], we perform pooling operation after FFN of VTE and then replace STE of our proposed method with it. The new architecture is termed as Pooling Transformer. The error increases by 0.4 mm, which highlights that our STE can preserve more valuable information than Pooling Transformer by exploiting local contexts to aggregate information. Removing VTE (only trained with single-frame loss) leads to a 1.1 mm increase in MPJPE error. Besides, removing STE (only trained with sequence loss), the MPJPE increases to 47.6 mm. These results validate the importance of both modules in our Strided Transformer, where VTE mainly models long-range information and STE focuses on aggregating information in a hierarchical global and local fashion.

### E. Qualitative Results

**Attention visualization.** Our method is easily interpretable through visualizing the attention score across frames to ex-

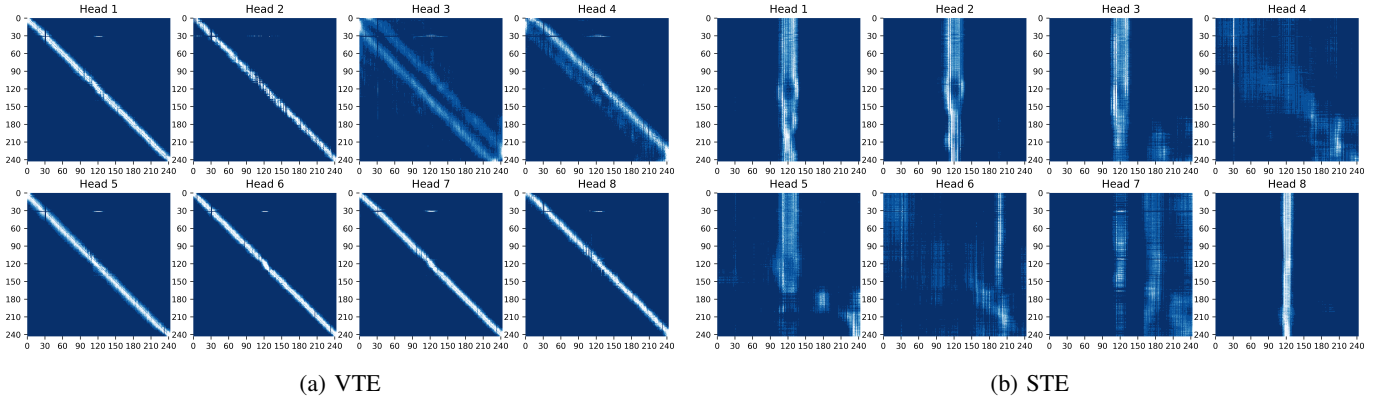


Fig. 8: Multi-head attention maps ( $h = 8$ ) from VTE and STE of our 243-frame model. It illustrates the self-attention mechanism systematically assigns a weight distribution to frames, all of which might contribute to the inference. The brighter color indicates stronger attention across frames.

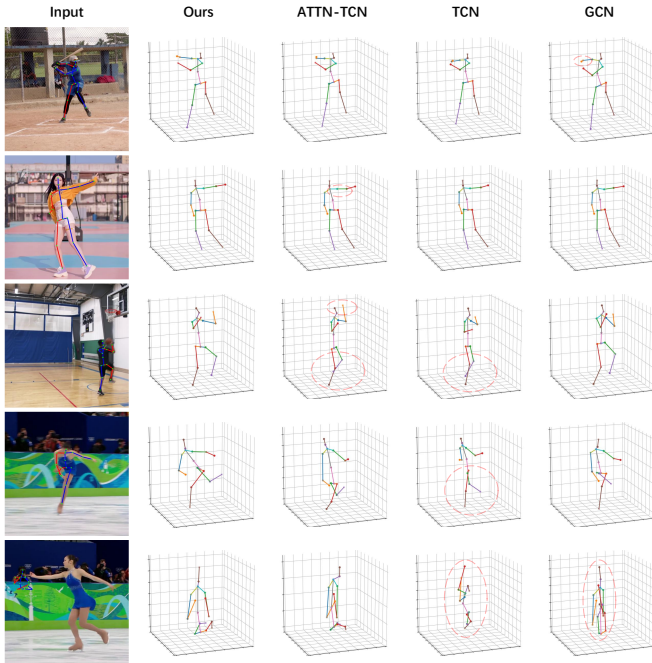


Fig. 9: Qualitative comparisons on challenging in-the-wild videos with previous state-of-the-art methods, ATTN-TCN [27], TCN [13], and GCN [17]. The last row shows the failure case, where the 2D detector has failed badly.

plain what temporal dependencies the target frame relies on. Visualization results of the multi-head attention maps of the first attention layers from VTE and STE (243-frame model) are shown in Fig. 8. The left map shows strong attention close to the input frames [58], [59], while the right map mainly pays strong attention to the target frame across all the sequences. This is expected since the proposed full-to-single strategy enables the VTE and STE modules to learn different representations: (i) VTE identifies important sequences that are close to the input frames selectively and enforces temporal consistency across frames. (ii) STE learns a specific representation from the input sequences using both past and future data

and improves the representation ability of features to reach an optimal inference for the target frame. Note that few attention head maps are sparse due to the different temporal patterns or semantics.

**3D reconstruction visualization.** We further evaluate our method on challenging in-the-wild videos from YouTube and the proposed 243-frame model can reach 108 FPS for real-time inference on a single GeForce RTX 2080 Ti GPU. Fig. 9 shows the qualitative comparisons with the previous state-of-the-art methods, ATTN-TCN [27], TCN [13], and GCN [17]. We use the same 2D detector (cascaded pyramid network [54]) to obtain 2D poses for a fair comparison and then fed them to the models. Despite the challenging samples with complex actions and fast movements, the proposed method can produce realistic and structurally plausible 3D predictions outperforming previous works. This demonstrates that our method is robust to partial occlusions and tolerant to depth ambiguity. The last row shows the failure case caused by a big 2D detection error.

## V. CONCLUSION

In this work, we investigate the suitability of applying a Transformer-based network to the task of video-based 3D human pose estimation. From the proposed Strided Transformer with strided Transformer encoder (STE) and full-to-single supervision scheme, we show how the representative single-pose representation can be learned from redundant sequences. The key is to reasonably use strided convolutions in the Transformer architecture to aggregate long-range information to a single-vector pose in a hierarchical global and local fashion. The computation cost can be reduced by a large margin. Moreover, a full-to-single supervision scheme is proposed to enforce temporal smoothness and further refine the estimation. Comprehensive experiments on two benchmark datasets demonstrate that our method achieves superior performance compared to state-of-the-art methods.

## REFERENCES

- [1] I. Radwan, A. Dhall, and R. Goecke, “Monocular image 3d human pose estimation under self-occlusion,” in *Proceedings of the IEEE*

- International Conference on Computer Vision (ICCV)*, 2013, pp. 1888–1895.
- [2] S. Li and A. B. Chan, “3d human pose estimation from monocular images with deep convolutional neural network,” in *Asian Conference on Computer Vision (ACCV)*, 2014, pp. 332–347.
  - [3] T. Zhao, S. Li, K. N. Ngan, and F. Wu, “3-d reconstruction of human body shape from a single commodity depth camera,” *IEEE Transactions on Multimedia*, vol. 21, no. 1, pp. 114–123, 2018.
  - [4] P. Hu, E. S.-I. Ho, and A. Munteanu, “3dbodynet: Fast reconstruction of 3d animatable human body shape from a single commodity depth camera,” *IEEE Transactions on Multimedia*, 2021.
  - [5] K. Pullen and C. Bregler, “Motion capture assisted animation: Texturing and synthesis,” in *Proceedings of the 29th annual conference on Computer graphics and interactive techniques*, 2002, pp. 501–508.
  - [6] P. Wang, W. Li, Z. Gao, C. Tang, and P. O. Ogunbona, “Depth pooling based large-scale 3-d action recognition with convolutional neural networks,” *IEEE Transactions on Multimedia*, vol. 20, no. 5, pp. 1051–1061, 2018.
  - [7] M. Liu, H. Liu, and C. Chen, “Robust 3d action recognition through sampling local appearances and global distributions,” *IEEE Transactions on Multimedia*, vol. 20, no. 8, pp. 1932–1947, 2017.
  - [8] M. Liu and J. Yuan, “Recognizing human actions as the evolution of pose estimation maps,” in *Proceedings of the IEEE Conference on Computer Vision and Pattern Recognition (CVPR)*, 2018, pp. 1159–1168.
  - [9] P. Wei, H. Sun, and N. Zheng, “Learning composite latent structures for 3d human action representation and recognition,” *IEEE Transactions on Multimedia*, vol. 21, no. 9, pp. 2195–2208, 2019.
  - [10] M. Garcia-Salguero, J. Gonzalez-Jimenez, and F.-A. Moreno, “Human 3d pose estimation with a tilting camera for social mobile robot interaction,” *Sensors*, vol. 19, no. 22, p. 4943, 2019.
  - [11] L. Gui, K. Zhang, Y. Wang, X. Liang, J. M. Moura, and M. Veloso, “Teaching robots to predict human motion,” in *Proceedings of the IEEE International Conference on Intelligent Robots and Systems (IROS)*, 2018, pp. 562–567.
  - [12] J. Martinez, R. Hossain, J. Romero, and J. J. Little, “A simple yet effective baseline for 3d human pose estimation,” in *Proceedings of the IEEE International Conference on Computer Vision (ICCV)*, 2017, pp. 2640–2649.
  - [13] D. Pavlo, C. Feichtenhofer, D. Grangier, and M. Auli, “3d human pose estimation in video with temporal convolutions and semi-supervised training,” in *Proceedings of the IEEE Conference on Computer Vision and Pattern Recognition (CVPR)*, 2019, pp. 7753–7762.
  - [14] G. Hua, W. Li, Q. Zhang, R. Ding, and H. Liu, “Weakly-supervised cross-view 3d human pose estimation,” *arXiv preprint arXiv:2105.10882*, 2021.
  - [15] K. Lee, I. Lee, and S. Lee, “Propagating lstm: 3d pose estimation based on joint interdependency,” in *Proceedings of the European Conference on Computer Vision (ECCV)*, 2018, pp. 119–135.
  - [16] M. Rayat Imtiaz Hossain and J. J. Little, “Exploiting temporal information for 3d human pose estimation,” in *Proceedings of the European Conference on Computer Vision (ECCV)*, 2018, pp. 68–84.
  - [17] Y. Cai, L. Ge, J. Liu, J. Cai, T.-J. Cham, J. Yuan, and N. M. Thalmann, “Exploiting spatial-temporal relationships for 3d pose estimation via graph convolutional networks,” in *Proceedings of the IEEE International Conference on Computer Vision (ICCV)*, 2019, pp. 2272–2281.
  - [18] A. Vaswani, N. Shazeer, N. Parmar, J. Uszkoreit, L. Jones, A. N. Gomez, L. u. Kaiser, and I. Polosukhin, “Attention is all you need,” in *Advances in Neural Information Processing Systems (NIPS)*, 2017, pp. 5998–6008.
  - [19] Y. Tay, M. Dehghani, D. Bahri, and D. Metzler, “Efficient transformers: A survey,” *arXiv preprint arXiv:2009.06732*, 2020.
  - [20] D. Zihang, L. Guokun, Y. Yiming, and Q. L. V., “Funnel-transformer: Filtering out sequential redundancy for efficient language processing,” in *Advances in Neural Information Processing Systems (NIPS)*, 2020.
  - [21] K. Han, Y. Wang, H. Chen, X. Chen, J. Guo, Z. Liu, Y. Tang, A. Xiao, C. Xu, Y. Xu *et al.*, “A survey on visual transformer,” *arXiv preprint arXiv:2012.12556*, 2020.
  - [22] S. He, H. Luo, P. Wang, F. Wang, H. Li, and W. Jiang, “Transreid: Transformer-based object re-identification,” *arXiv preprint arXiv:2102.04378*, 2021.
  - [23] X. Li, Y. Hou, P. Wang, Z. Gao, M. Xu, and W. Li, “Trear: Transformer-based rgb-d egocentric action recognition,” *arXiv preprint arXiv:2101.03904*.
  - [24] L. Han, P. Wang, Z. Yin, F. Wang, and H. Li, “Exploiting better feature aggregation for video object detection,” in *Proceedings of the 28th ACM International Conference on Multimedia (ACMMM)*, 2020, pp. 1469–1477.
  - [25] X. Li, Y. Hou, P. Wang, Z. Gao, M. Xu, and W. Li, “Transformer guided geometry model for flow-based unsupervised visual odometry,” *Neural Computing and Applications*, pp. 1–12, 2021.
  - [26] M. Geva, R. Schuster, J. Berant, and O. Levy, “Transformer feed-forward layers are key-value memories,” *arXiv preprint arXiv:2012.14913*, 2020.
  - [27] R. Liu, J. Shen, H. Wang, C. Chen, S.-c. Cheung, and V. Asari, “Attention mechanism exploits temporal contexts: Real-time 3d human pose reconstruction,” in *Proceedings of the IEEE Conference on Computer Vision and Pattern Recognition (CVPR)*, 2020, pp. 5064–5073.
  - [28] C. Ionescu, D. Papava, V. Olaru, and C. Sminchisescu, “Human3.6m: Large scale datasets and predictive methods for 3d human sensing in natural environments,” *IEEE Transactions on Pattern Analysis and Machine Intelligence*, vol. 36, no. 7, pp. 1325–1339, 2013.
  - [29] L. Sigal, A. O. Balan, and M. J. Black, “Human3.6m: Synchronized video and motion capture dataset and baseline algorithm for evaluation of articulated human motion,” *International Journal of Computer Vision*, vol. 87, no. 12, pp. 4–27, 2010.
  - [30] G. Pavlakos, X. Zhou, K. G. Derpanis, and K. Daniilidis, “Coarse-to-fine volumetric prediction for single-image 3d human pose,” in *Proceedings of the IEEE Conference on Computer Vision and Pattern Recognition (CVPR)*, 2017, pp. 7025–7034.
  - [31] X. Sun, B. Xiao, F. Wei, S. Liang, and Y. Wei, “Integral human pose regression,” in *Proceedings of the European Conference on Computer Vision (ECCV)*, 2018, pp. 529–545.
  - [32] L. Zhao, X. Peng, Y. Tian, M. Kapadia, and D. N. Metaxas, “Semantic graph convolutional networks for 3d human pose regression,” in *Proceedings of the IEEE Conference on Computer Vision and Pattern Recognition (CVPR)*, 2019, pp. 3425–3435.
  - [33] J. Liu, H. Ding, A. Shahroudy, L.-Y. Duan, X. Jiang, G. Wang, and A. C. Kot, “Feature boosting network for 3d pose estimation,” *IEEE Transactions on Pattern Analysis and Machine Intelligence*, vol. 42, no. 2, pp. 494–501, 2019.
  - [34] H.-S. Fang, Y. Xu, W. Wang, X. Liu, and S.-C. Zhu, “Learning pose grammar to encode human body configuration for 3d pose estimation,” in *Thirty-Second AAAI Conference on Artificial Intelligence*, 2018.
  - [35] T. Xu and W. Takano, “Graph stacked hourglass networks for 3d human pose estimation,” in *Proceedings of the IEEE Conference on Computer Vision and Pattern Recognition (CVPR)*, 2021, pp. 16 105–16 114.
  - [36] J. Wang, S. Yan, Y. Xiong, and D. Lin, “Motion guided 3d pose estimation from videos,” *arXiv preprint arXiv:2004.13985*, 2020.
  - [37] N. Carion, F. Massa, G. Synnaeve, N. Usunier, A. Kirillov, and S. Zagoruyko, “End-to-end object detection with transformers,” in *European Conference on Computer Vision (ECCV)*, 2020, pp. 213–229.
  - [38] X. Zhu, W. Su, L. Lu, B. Li, X. Wang, and J. Dai, “Deformable detr: Deformable transformers for end-to-end object detection,” *arXiv preprint arXiv:2010.04159*, 2020.
  - [39] A. Dosovitskiy, L. Beyer, A. Kolesnikov, D. Weissenborn, X. Zhai, T. Unterthiner, M. Dehghani, M. Minderer, G. Heigold, S. Gelly *et al.*, “An image is worth 16x16 words: Transformers for image recognition at scale,” *arXiv preprint arXiv:2010.11929*, 2020.
  - [40] L. Yuan, Y. Chen, T. Wang, W. Yu, Y. Shi, F. E. Tay, J. Feng, and S. Yan, “Tokens-to-token vit: Training vision transformers from scratch on imagenet,” *arXiv preprint arXiv:2101.11986*, 2021.
  - [41] K. Lin, L. Wang, and Z. Liu, “End-to-end human pose and mesh reconstruction with transformers,” *arXiv preprint arXiv:2012.09760*, 2020.
  - [42] C. Zheng, S. Zhu, M. Mendieta, T. Yang, C. Chen, and Z. Ding, “3d human pose estimation with spatial and temporal transformers,” *arXiv preprint arXiv:2103.10455*, 2021.
  - [43] K. Gong, J. Zhang, and J. Feng, “Poseaug: A differentiable pose augmentation framework for 3d human pose estimation,” in *Proceedings of the IEEE Conference on Computer Vision and Pattern Recognition (CVPR)*, 2021, pp. 8575–8584.
  - [44] J. Lin and G. H. Lee, “Trajectory space factorization for deep video-based 3d human pose estimation,” *arXiv preprint arXiv:1908.08289*, 2019.
  - [45] J. Xu, Z. Yu, B. Ni, J. Yang, X. Yang, and W. Zhang, “Deep kinematics analysis for monocular 3d human pose estimation,” in *Proceedings of the IEEE Conference on Computer Vision and Pattern Recognition (CVPR)*, 2020, pp. 899–908.
  - [46] A. Zeng, X. Sun, F. Huang, M. Liu, Q. Xu, and S. Lin, “Srnet: Improving generalization in 3d human pose estimation with a split-and-recombine approach,” in *European Conference on Computer Vision (ECCV)*, 2020, pp. 507–523.
  - [47] T. Chen, C. Fang, X. Shen, Y. Zhu, Z. Chen, and J. Luo, “Anatomy-aware 3d human pose estimation with bone-based pose decomposition,” *IEEE Transactions on Circuits and Systems for Video Technology*, 2021.

- [48] G. Pavlakos, X. Zhou, and K. Daniilidis, “Ordinal depth supervision for 3d human pose estimation,” in *Proceedings of the IEEE Conference on Computer Vision and Pattern Recognition (CVPR)*, 2018, pp. 7307–7316.
- [49] K. Liu, R. Ding, Z. Zou, L. Wang, and W. Tang, “A comprehensive study of weight sharing in graph networks for 3d human pose estimation,” in *Proceedings of the European Conference on Computer Vision (ECCV)*, 2020, pp. 318–334.
- [50] X. Chen, K.-Y. Lin, W. Liu, C. Qian, and L. Lin, “Weakly-supervised discovery of geometry-aware representation for 3d human pose estimation,” in *Proceedings of the IEEE Conference on Computer Vision and Pattern Recognition (CVPR)*, 2019, pp. 10 895–10 904.
- [51] D. Tome, M. Toso, L. Agapito, and C. Russell, “Rethinking pose in 3d: Multi-stage refinement and recovery for markerless motion capture,” in *2018 International Conference on 3D Vision (3DV)*, 2018, pp. 474–483.
- [52] M. Kocabas, S. Karagoz, and E. Akbas, “Self-supervised learning of 3d human pose using multi-view geometry,” in *Proceedings of the IEEE Conference on Computer Vision and Pattern Recognition (CVPR)*, 2019, pp. 1077–1086.
- [53] Y. Cheng, B. Yang, B. Wang, W. Yan, and R. T. Tan, “Occlusion-aware networks for 3d human pose estimation in video,” in *Proceedings of the IEEE International Conference on Computer Vision (ICCV)*, 2019, pp. 723–732.
- [54] Y. Chen, Z. Wang, Y. Peng, Z. Zhang, G. Yu, and J. Sun, “Cascaded pyramid network for multi-person pose estimation,” in *Proceedings of the IEEE Conference on Computer Vision and Pattern Recognition (CVPR)*, 2018, pp. 7103–7112.
- [55] K. He, G. Gkioxari, P. Dollár, and R. Girshick, “Mask r-cnn,” in *Proceedings of the IEEE international conference on computer vision (ICCV)*, 2017, pp. 2961–2969.
- [56] R. Dabral, A. Mundhada, U. Kusupati, S. Afaq, A. Sharma, and A. Jain, “Learning 3d human pose from structure and motion,” in *Proceedings of the European Conference on Computer Vision (ECCV)*, 2018, pp. 668–683.
- [57] A. Newell, K. Yang, and J. Deng, “Stacked hourglass networks for human pose estimation,” in *Proceedings of the European Conference on Computer Vision (ECCV)*, 2016, pp. 483–499.
- [58] Z. Wu, Z. Liu, J. Lin, Y. Lin, and S. Han, “Lite transformer with long-short range attention,” in *International Conference on Learning Representations (ICLR)*, 2020.
- [59] Z. Jiang, W. Yu, D. Zhou, Y. Chen, J. Feng, and S. Yan, “Convbert: Improving bert with span-based dynamic convolution,” in *Advances in Neural Information Processing Systems (NIPS)*, 2020.

## VI. APPENDIX



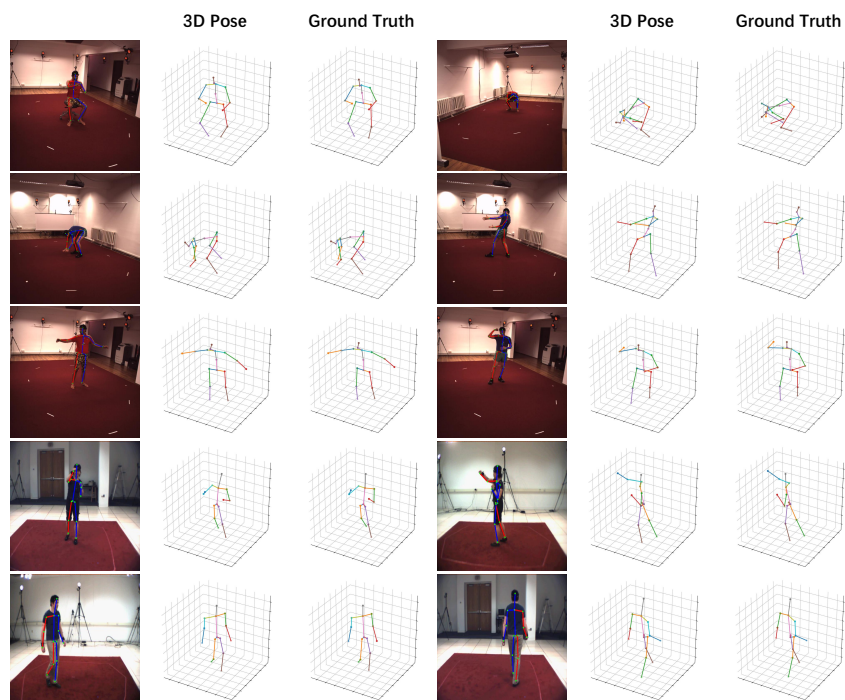


Fig. 10: Visual results of our proposed method on Human3.6M dataset (first 3 rows) and HumanEva-I dataset (last 2 rows).

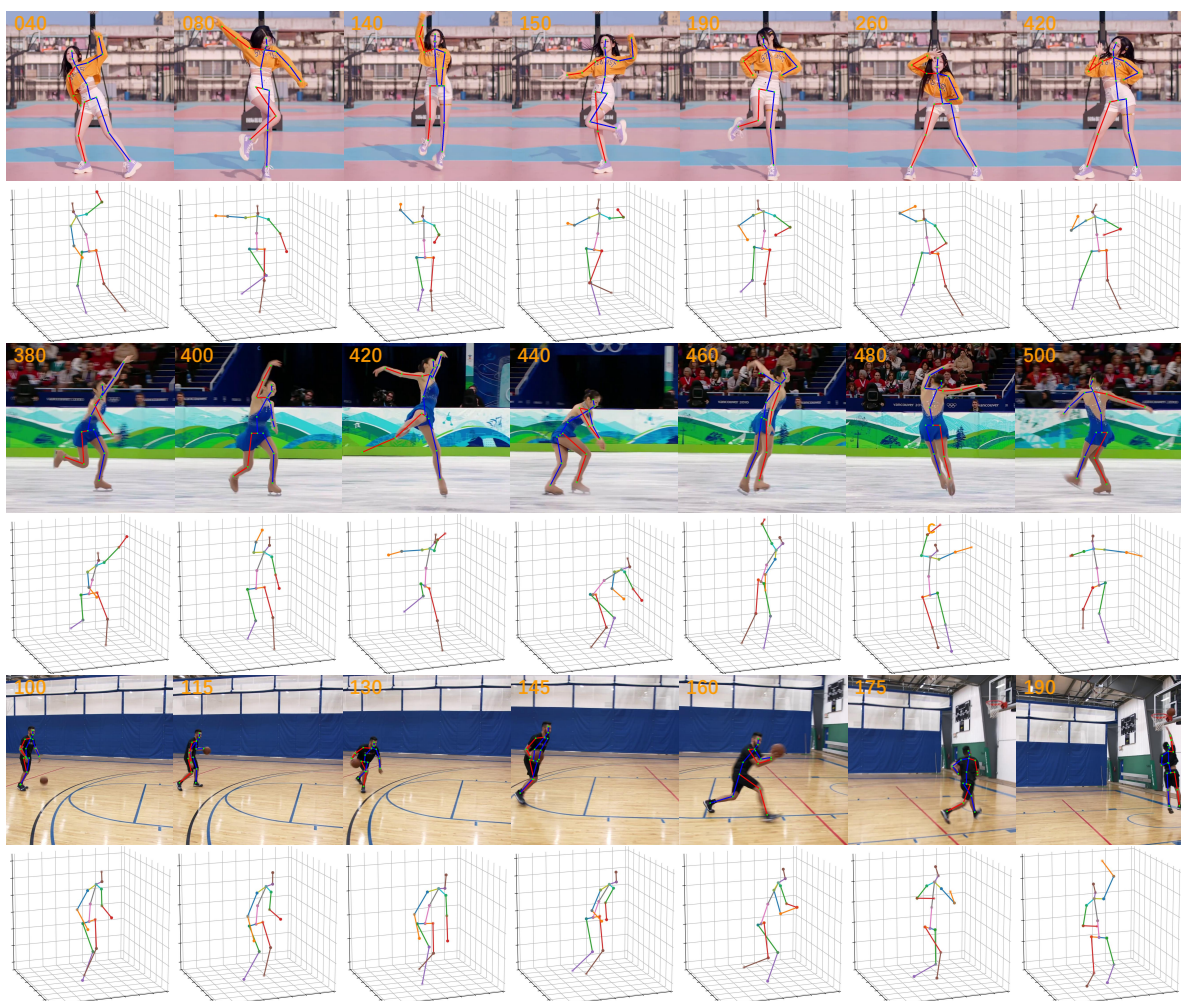


Fig. 11: Qualitative results on challenging wild videos. The number is the frame index of input videos.